

HYDROGEL MICROCHANNEL FABRICATION USING LASER MICRODISSECTION TECHNOLOGY

A Dissertation
Presented to
The Academic Faculty

by

Kathryn Castro-Quilang

In Partial Fulfillment
of the Requirements for the Degree
Master of Science in the
School of Biomedical Engineering

Georgia Institute of Technology
August 2023

COPYRIGHT © 2023 BY KATHRYN CASTRO-QUILANG

HYDROGEL MICROCHANNEL FABRICATION USING LASER MICRODISSECTION TECHNOLOGY

Approved by:

Dr. Ankur Singh, Advisor
Wallace H. Coulter Department of
Biomedical Engineering
Georgia Institute of Technology

Dr. Brandon Dixon
George W. Woodruff School of
Mechanical Engineering
Georgia Institute of Technology

Dr. Ahmet Coskun
Wallace H. Coulter Department of
Biomedical Engineering
Georgia Institute of Technology

Dr. Aniruddh Sarkar
Wallace H. Coulter Department of
Biomedical Engineering
Georgia Institute of Technology

Date Approved: July 27, 2023

ACKNOWLEDGEMENTS

I would like to express my utmost gratitude to Dr. Ankur Singh for supporting me through my MS journey and for the research opportunity in the immunotherapy and cell engineering laboratory. I would like to thank the members of the immunotherapy and cell engineering laboratory for their technical aid and suggestions throughout this project.

Thank you to my good friends I met upon starting this master's program: Aolani, Kendra, Anushka, Zach, and Charles. Not only did they motivate and support me through this journey, but they also became my second family.

Finally, I would like to thank my sister, Kristine, and my parents, Fernando and Cynthia, for developing my character and helping me build strength to accomplish what I set out to do. Their constant, unconditional love motivates me every day to be a good person, and I am forever grateful.

TABLE OF CONTENTS

ACKNOWLEDGEMENTS	iii
TABLE OF CONTENTS	iv
LIST OF TABLES	vi
LIST OF FIGURES	vii
LIST OF SYMBOLS AND ABBREVIATIONS	viii
SUMMARY	ix
CHAPTER 1. Introduction	1
1.1 Immunology Background and Lymphatic Physiology	1
1.1.1 Lymphatic Vasculature Pathology	2
1.2 In Vitro Vasculature Modeling	3
1.2.1 Microfluidic models	4
1.2.2 Hydrogels in Lymphatics Models	5
1.2.3 Current Complications	7
CHAPTER 2. Laser Microdissection	7
2.1 ZEISS PALM MicroBeam Laser Microdissection	7
2.2 Expanded Direction of Laser Microdissection	9
2.2.1 Vasculature	9
2.2.2 Gut System	10
2.3 Proposed Work and Hypothesis	10
CHAPTER 3. Property Optimizations Before development of Lymphatics Vasculature	12
3.1 Hydrogel Optimization	12
3.1.1 Peg-Acrylate	12
3.1.2 Alginate	13
3.1.3 GelMA	14
3.1.4 Results and Weight Percentage	14
3.2 Microfluidic Device Design	16
3.2.1 Serpentine Device	16
3.2.2 Three-Channel device	17
3.2.3 Results	17
3.3 Laser Cutting Optimization	19
3.3.1 Microscope Properties	19
3.3.2 Laser Properties	20
CHAPTER 4. Development of Lymphatic Vasculature	22

4.1	Weight percentage	22
4.2	Channel Cuts	25
4.2.1	Simple Channels	25
4.2.2	Branched Network	25
4.2.3	Lymphatic Channels	26
4.2.4	Perfusion with Cells	27
CHAPTER 5.	Methods	30
5.1	Hydrogel Preparation	30
5.2	Microfluidic Device Creation	31
5.3	LCM	31
5.3.1	Optimization of Laser Cut and Catapult Settings	31
5.3.2	LCM Cutting and Perfusion Procedure	32
CHAPTER 6.	Conclusions and Future Directions	34
APPENDIX A.	Supplemental Images	35
A.1	Bubble Formation during Photoablation Process	35
A.2	Channel Closing during Photoablation Process	36
A.3	Inlet and Outlet Close during Photoablation Process	36
A.4	Long Laser Cuts in Three-Channel Device During Photoablation Process	37

LIST OF TABLES

Table 1 Microfluidic Device Dimensions.....	19
Table 2 Optimized Settings for ZEISS PALM LCM Technology	21
Table 3 Channel dimensions of laser ablated channels at varied GelMA weight percentage.	24
Table 4 Dimensions of laser ablations of various cut designs	27

LIST OF FIGURES

Figure 1 Lymphatic vasculature in (a) healthy cases and (b) malformed cases	3
Figure 2 Current use of Laser Capture Microdissection of isolation of cell populations... ..	8
Figure 3 Proposed use of LCM Technology to ablate channels in hydrogel that allow for perfusion.	11
Figure 4 The chemical structures and associated photoablations of (a) GelMA, (b) PEG-4-Acrylate, and (c) Alginate. GelMA formed defined cuts, PEG-Acrylate formed bubbles, and Alginate did not respond to LCM ablations. The z-formation patterns in Alginate are cuts on the device, not the hydrogel itself showing incompatibility of Alginate with LCM.	15
Figure 5 (a) Microfluidic device preparation procedure before performing photoablation. Tiled brightfield images of the microfluidic pattern design of the (b) Serpentine Device and (c) Three-Channel Device	18
Figure 6 Brightfield images of laser ablated channels and perfusion of FITC through channels of GelMA at (a) 5 wt/v% (b) 10 wt/v% (c) 15 wt/v% and (d) 20 wt/v%	23
Figure 7 Various laser ablations at 20 wt/v% GelMA and associated perfusion with FITC coated beads through (a) simple channel, (b) branched channel, (c) single malformation channel, and (d) triple malformation channel.	26
Figure 8 Perfusion of a (a) simple channel and (b) malformation with lymphocytes tagged with Cell Tracker Red and associated brightfield image of laser ablations.....	28

LIST OF SYMBOLS AND ABBREVIATIONS

LEC	Lymphatic Endothelial Cell
ECM	Extracellular Matrix
GelMA	Gelatin Methacryol
PEG	Polyethylene Glycol
LCM	Laser Capture Microdissection
PALM	Precision Laser Microdissection
LAP	Lithium Acylphosphonate
FITC	Fluorescein Isothiocyanate-dextran
PDMS	Polydimethylsioxane
DTT	Dithiothreitol

SUMMARY

Lymphatic vasculature plays a critical role in immune system function, including a major role in facilitating transport of antigens and immune cells through the lymphatic fluid. While microfluidic chip models have been extensively used to study lymphatic vessels, using hydrogels to closely mimic in vivo environments by free-forming lymphatic network features and exploring patterned lymphatic networks, has seen limited research. This study investigates the potential of laser capture dissection technology, specifically utilizing photoablation settings, to create channels in microfluidic systems that emulate structural aspects of lymphatic vasculature. Through optimizations of hydrogel properties, microfluidic designs, and ZEISS PALM MicroBeam Laser Microdissection settings, well-defined patterned channels achieve flow and perfusion. The application of LCM technology holds significant promise for various lymphatic and vascular modeling applications, including tissue engineering, system or organ-on-chip platforms, and organoid models.

CHAPTER 1. INTRODUCTION

1.1 Immunology Background and Lymphatic Physiology

The lymphatic vasculature is an integral part of the immune system, though it is not formally considered part of the immune system. Among its immunological roles, one major role involves trafficking antigens and immune cells throughout the lymphatic system lumens via lymph fluid[1]. Lymphatics employ a one-way transport mechanism whereby fluid and proteins collected from the interstitial space are transported to various locations and subsequently returned to the blood circulation. The lymphatic vasculature is organized in two major compartments: initial lymphatics and collecting lymphatics. The sizes of these conduits range from 10 μm to 2 mm in diameter[2]. Fluid travels from capillaries into the interstitium, forming interstitial fluid or lymph. The lymph subsequently exits the interstitial space by draining into initial lymphatics [3]. These afferent vessels transport and drain lymph into a network of sinuses within lymph nodes, an immune organ responsible for the recognition of foreign antigens, the development of long-lasting adaptive immune responses to antigens, and the induction of pathogen elimination[3]. Collecting, efferent lymphatic vessels exit lymph nodes, drain into progressively larger trunks, or ducts, which finally join a large vein, returning lymph to the blood circulatory system and completing the cycle[2]. This lymph cycle accomplishes many functions to maintain systemic health, including fluid drainage from extracellular spaces, intestinal tract lipid absorption, maintenance of fluid homeostasis, and transportation of lymphocytes and antigen-presenting cells. [1-3]

Lymphatic vessels are organized by multiple components: an inner monolayer of lymphatic endothelial cells (LECs), intraluminal valves, a collagen basement membrane, and, in larger vessels, an outer smooth muscle cell cover[2, 3]. Lymph formation and flow are initially dependent on hydrostatic and osmotic pressure differences between the interstitial and lymphatic vessel fluid[2], and subsequent intraluminal pressure differences propel the fluid flux in the intended direction of lymph flow. Vessel pressure gradients develop primarily due to tissue movement, which along with intravascular one-way valves, drives fluid flow in the desired direction while resisting leaking or back flow. Flow is also thought to be regulated by contractile properties of larger collecting vessels[4]. Adjacent muscle cells are highly specialized to provide contractions that promote unidirectional transport of lymph along the length of vessels. The primary function of these muscle cells is to generate the necessary pressure to pump lymph against gradually increasing pressure, and adapting pumping activity to increases in interstitial fluid load, vascular lymph, and increased inflammatory mediators. Although the flow of interstitial fluid has an impact on immunity, it is only occasionally discussed in the field of immunology[2-4].

1.1.1 Lymphatic Vasculature Pathology

Defects in lymphatic vasculature, congenital or acquired, can give rise to immunological pathology. Malformations in lymphatics can present in multiple forms including Lymphoedema, lymph formation and adsorption imbalance in vessels; Lymphangitis, lymphatic vessel inflammation; Lymphangioma, benign neoplasm of lymphatic vessels; and Lymphangiosarcoma, malignant neoplasm of lymphatic vessels. Furthermore, lymphatics play a major role in the metastasis of cancer, and dissemination of immune system malignancies such as lymphomas.[5] The majority of defects cause

morphologic changes in the lymphatic vasculature, i.e., lymphatic malformations. These lymphatic anomalies present as localized or multifocal lesions of lymphatic vasculature that range from small discolorations to large deformations and infiltrative masses[6]. Oncogenic mutations can lead to these malformations by acting as lymphatic endothelial cell-autonomous drivers. The mutations lead to pro-lymphangiogenic activity that promotes progressive malformed lymphatic overgrowth depicted in the diagram in **Figure 1**[5, 6]. Although there is significant morphologic variability in lymphatic vasculature in healthy states [5, 6] lymphatic malformations (LM) exhibit major differences in channel sizes, which can be classified as microcystic, macrocystic, or a combination of both. Macrocystic formations are distinguished from microcystic dilations by being of sufficient size that they can be effectively treated using macroscopic surgical techniques.[7]



Figure 1 Lymphatic vasculature in (a) healthy cases and (b) malformed cases

1.2 In Vitro Vasculature Modeling

Compared to experimental models to study blood vasculature, there are fewer designs that have been developed to explore the lymphatics[8]. However, this area of research has been attractive due to lymphatic involvement in numerous diseases. Lymphatic vasculature dysfunction is involved in numerous diseases and cancer metastasis, therefore, the ability to recapitulate lymphatics in 2D and 3D in vitro models

would aid in therapeutic developments[9]. Ex vivo and in vitro engineered systems to model lymphatic vasculature have been developed and utilized, including isolated vessels, cell culturing methods in petri dishes, culture flasks, and trans-well plates, organ-on-chip, bioprinting, and engineered 3D microenvironments[10]. Although LECs cultured in 2D systems have provided information on biochemical processes and signaling, 3D microenvironments and more advanced methods better mimic the in vivo habitat and the biomechanical cues that affect signaling pathways, migration properties, and growth among other biological structures[8-10]. 3D in vitro models include extracellular matrix (ECM) scaffolds, or cell culture embedded in ECM, organoids or spheroids, and microfluidic chips.

1.2.1 Microfluidic models

The development of microcirculation-on-chip or organ-on-chip models that integrated lymphatic vasculature has been expected to provide insight in therapeutic compounds, drug delivery, and exploration of tumor invasion and metastasis[8-11]. Designs of microfluidic models for vasculature studies have been utilized to encourage angiogenesis or lymphangiogenic applications. Endothelial cells are cultured within the device, and the design of the microfluidics, in some cases, encourages sprouting and thus vasculature growth. These models allow for exploration of LEC communication and behavior within an organ-on-chip system[8]. These microfluidic designs generally consisted of multiple channels cultured with specialized cells such that behavior and cell-cell communication between these channels can be analyzed. Preformed lymphatic vasculature that was then perfused with LECs, and lymph has been explored significantly less. Due to the complexity of the lymphatic fluidic and mechanical environment,

engineered lymphatic vasculature and tissue have been mostly simplified models, where the main goal is the formation of vessels and structures close to in vivo morphology[9]. The microfluidic channel designs that have been utilized to mimic the lymphatic vessel have been simple channel designs and some utilized material, such as PDMS, that lacks biomechanical properties of the in vivo habitat.

1.2.2 Hydrogels in Lymphatics Models

Hydrogels are an appealing specialized class of biomaterials that are characterized by their viscoelasticity. Hydrogels are mostly liquid in content and have both liquid and solid behavior. Crosslinking density, polymer alignment, stiffness, and degradation can be adjusted in hydrogels allowing for control over properties to mimic the lymphatic microenvironment, enhance cellular performance, and aid in other functions[11]. The utilization of hydrogel systems has also been appealing to the delivery of therapies, especially that of restoring lymphatic function, and has been beneficial to mimic in vivo microenvironments and mechanics in vasculature models[9, 11]. Hydrogels can mimic the properties of the ECM and improve cell adhesion and functionality. Microfluidic chips have been loaded with hydrogels and cells to reflect a physiologically similar tissue-like model. Hydrogels commonly used for lymphatic vessel-on-chip and microcirculation-on-chip devices include Collagen types, Matrigel, Gelatin Methacryloyl (GelMA), and Polyethylene glycol (PEG) hydrogels[11]. Hydrogels would encapsulate extravascular and ECM cells to form a microenvironment and lymphatics would be in a separate reservoir or channel yet allowed to interact with the hydrogel microenvironment. This allowed for the analysis of lymphatic involvement with the hydrogel microenvironment[9, 11].

Recent developments in hydrogel strategies to encourage the growth of lymphatics, either for regenerative purposes or as model system to study lymphatic biology, is novel and in early stages of research. Programmable hydrogels to regenerate the lymphatic system, modulate inflammation, and enhance immunotherapy have been explored.[12] PEG-4-MAL (4-arm PEG Methacrylate) has been investigated to regulate lymphatic sprouting. Among the many variables that influenced lymphatic sprouting, matrix stiffness was evaluated. Overall, PEG-4MAL hydrogels were utilized to study lymphatic function, responsiveness to interventions, and their possible in-vivo application.[13] Other studies explored the compatibility of lymphatic cells in hydrogel systems.[14] The feasibility of reconstructing lymph vessels using LECs in conjunction with polyglycolic acid (PGA) scaffolds was tested. It was demonstrated that LECs effectively served as seed cells and were successfully combined with PGA scaffolds, resulting in a tissue-engineered tubular structure that exhibited preliminary characteristics of lymph vessels. It indicated the potential for constructing tissue-engineered lymph vessels with LECs and hydrogels.[15] Fibrin scaffolds were also utilized in studying network formation of LECs and blood vascular endothelial cells (BECs)[16].

Hydrogels used within lymphatic circulation on chip models have been explored using a variety of methods. One study demonstrated lymphatic and blood capillary morphogenesis within fibrin gels, comparing flow with static conditions. The model was a multichamber fluidic system studying cell migration, contractile cells such as fibroblasts, and multicellular cultures, all under the influence of interstitial flow [17]. Studies have developed cellular lined conduits within hydrogel to develop a vessel-on-chip. Rods were introduced in the hydrogel and removed after crosslinking and cells lined the conduit

forming a single vessel on chip [18]. Similarly, a lymphatic vessel-on-chip was developed in a similar fashion and seeded with LECs [19]. However, these models of cell lined vasculature are simple, single channels.

1.2.3 Current Complications

Lymphatic vessels can be studied utilizing microfluidic chip models. However, these models can be improved to more closely mimic lymphatic vessels in normal and diseased states, by precisely controlling lymphatic vascular patterning with cellular loading to encourage lined conduits. Although the interactions of LECs and lymphatics with respect to lymphangiogenesis and lymphatic impact within an organ can be modeled using the designs mentioned in the prior section, the formation of more complex lymphatic network structures within the material that mimics in vivo habitats, such as hydrogels, has scarcely been explored. Furthermore, flow and perfusion of such patterned lymphatic vessels have been minimally studied[8-11].

CHAPTER 2. LASER MICRODISSECTION

2.1 ZEISS PALM MicroBeam Laser Microdissection

Laser-capture microdissection (LCM) is a method to obtain subpopulations of tissue cells under microscopic visualization. LCM can isolate cells of interest directly by cutting the boundary of the cell and separating it from unwanted cells or tissue. This results in histologically pure enriched cell populations. Following isolation, downstream applications can be applied such as DNA sequencing, RNA expression profiling, proteomics, and genetic studies.[20]

ZEISS PALM MicroBeam Laser Microdissection is a specific LCM system and highly advanced technology used in the field of molecular biology and histopathology. PALM (Precision Laser Microdissection) system consists of a microscope integrated with a laser microdissection device. ZEISS PALM LCM utilizes photoablation for laser-capture techniques in which material removal is through controlled interaction of light energy with the target material. Laser radiation ablates or vaporizes the material without thermal damage to the surrounding area. Laser energy is absorbed by the material, leading to the rapid heating and vaporization of the targeted, microscopic area. This process occurs on a very short timescale, picoseconds or femtoseconds. ZEISS PALM LCM combines high-resolution microscope visualization and capabilities and laser parameters for precise photoablation. Laser parameters include laser energy or intensity, laser focus, pulse duration and speed, and repetition rate. Collection of the sample utilizes the same photoablation technology to “catapult” the sample into a collection vial. The laser defocuses and detaches the cells or region guiding the isolated sample to a collection cap without contamination of the surrounding sample.

Typical uses of LCM allow researchers to study specific cell populations or tissue regions, providing valuable insights into various biological processes, such as cancer

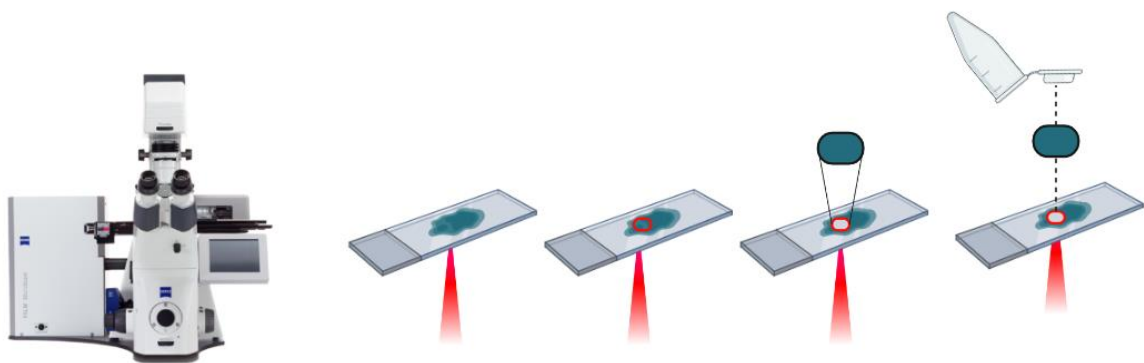


Figure 2 Current use of Laser Capture Microdissection of isolation of cell populations.

progression, tissue development, and cellular interactions. This is achievable through photoablation of isolated cell populations with the laser, and sterile collection of isolated samples. Further experimentation on isolated cells is commonly performed by researchers. This process is highlighted in **Figure 2**.

2.2 Expanded Direction of Laser Microdissection

While laser-capture technology is predominantly used for the isolation of tissue or cell populations, this technology, particularly the photoablation setting, has been explored for other applications. The ablation of hydrogels within a microfluidic chip to produce a microcirculation-on-chip model has been explored. These models would allow for enhanced imitation of morphological and biomechanical physiology, particularly to vasculature and other conduits.

2.2.1 Vasculature

There have been limited publications on laser-capture technology as a means of producing physiologically similar vasculature. Brandenburg, et al. employed laser photoablation to fabricate functional 3D microfluidic networks[21]. The fabrication began with a proof of perfusion utilizing a PDMS mount filled with polyethylene glycol (PEG) hydrogels. The design of the mount contained a section to hold the hydrogel while filling one side of the hydrogel with media. This microfluidic design would allow the hydrogel to undergo laser photoablation and produce a channel-inducing perfusion of media through the hydrogel into another reservoir. This would prove the possibility of photoablation as a useful technology for microfluidic channel fabrication. More complex networks of

channels were fabricated that mimicked the capillary bed networks and were perfused with fluorescent dye.[21]

Laser photoablation of microchannels in hydrogels was performed for directed neural cell growth. The laser properties and biomaterial properties on microchannel formation were characterized in PEGylated fibrinogen hydrogels and the effect of photoablation on cellular outgrowth. The pulsed laser generated guidance structures in the hydrogels that were predominantly single-channel simple structures. While this study did not utilize the ZEISS PALM LCM system, a similar laser photoablation technology provided nanosecond and femtosecond laser pulses to produce characterizable channels.[22]

2.2.2 *Gut System*

Increased complexity of conduits and vasculature have been explored using LCM. Nikolaev, et al. developed a microfluidic device whereby a microglial gut system was photoablated and perfused with specialized gut cells. The generation of the microchannels in this gut-on-chip system used nanosecond pulses with the ZEISS PALM LCM technology on Matrigel hydrogels. The microscale model of the gut allowed for cells to attach to the walls of the ablated glial conduit forming a long-term homeostatic culture of tubular mini-guts. [23]

2.3 **Proposed Work and Hypothesis**

It is postulated that photoablation through ZEISS PALM LCM technology could produce a microfluidic system to mimic lymphatic vasculature structure. Hydrogels would be utilized to assimilate biomechanical properties of the in vivo microenvironment while

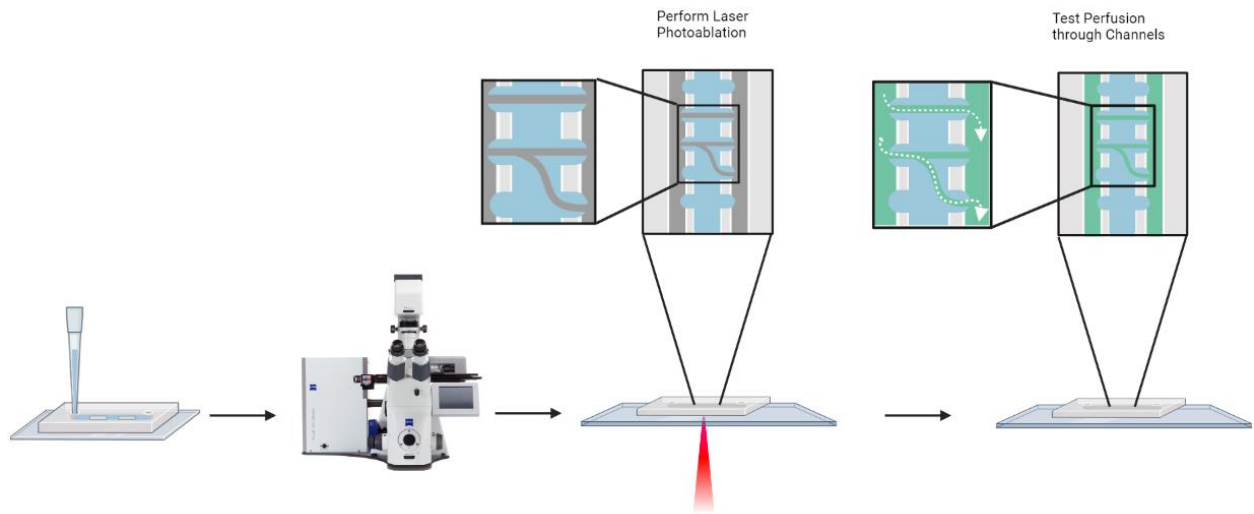


Figure 3 Proposed use of LCM Technology to ablate channels in hydrogel that allow for perfusion.

patterned laser cutting would produce morphologies approximating vasculature. The photoablation procedure could be extended to lymphatics patterning in a 2D model. Extended study in interstitial flow and utilizing immune cells to add to the model will further enhance the lymphatic model. **Figure 3** describes the process to achieve the microfluidic model and the proposed work with photoablation.

CHAPTER 3. PROPERTY OPTIMIZATIONS BEFORE DEVELOPMENT OF LYMPHATICS VASCULATURE

3.1 Hydrogel Optimization

Hydrogels are appealing due to their biocompatibility and properties that mimic the biomechanics of tissue. Along with the appeal of the viscoelasticity and structural integrity of their 3D network, hydrogel material properties allow for the adherence of cells and proteins. However, the behavior of each hydrogel type is dependent on its respective chemistry. Polymer chemistry and crosslinking impacts properties such as mechanical strength, biocompatibility, biodegradability, swellability, and stimuli sensitivity. Therefore, hydrogels were examined to compare compatibility with photoablation, and channel formation that supports perfusion. In this study, perfusion was tested against two criteria: first, the reservoirs on each side of the channels or patterned networks are filled with dye, cells, or beads, and second, the dye, beads or cells are well-defined within the channels or conduits without leakage. Detailed methodology on preparation of the hydrogels, and photoablation procedure are discussed in the Methods section. Parameters of the laser photoablation, discussed in the Laser Cutting Optimization section, were troubleshooted and adjusted for each hydrogel.

3.1.1 Peg-Acrylate

PEG hydrogels are formed by crosslinking polyethylene glycol (PEG) chains through various chemical methods. PEG hydrogels possess several desirable properties, including high water content, tunable mechanical properties, biocompatibility, and

resistance to protein adsorption[24]. Their chemistry allows for precise control over crosslinking density, degradation rates, and the incorporation of bioactive molecules, making them attractive for a wide range of applications. PEG hydrogels are available in a wide range of molecular weights and end groups, such as maleimides, acrylates, and vinyl sulfones. Furthermore, PEGs can be multi-functionalized based on how many arms are available in the PEG group. Maleimides, acrylates, and vinyl sulfones are involved in Michael-type addition reactions with thiols to achieve hydrogel crosslinking. The addition of a nucleophile, in this case a thiol, to a carbon-carbon double bond is a Michael-type addition reaction. Mechanical and functional properties can be tuned by varying concentrations of crosslinker type and density, end group macromonomer type and density, and additional groups such as peptides.[24]

Laser photoablation was tested on 4 Arm PEG-Acrylate (PEG-4-Acrylate, Sigma Aldrich JKA7034-1G). Both ease and compatibility with the technology were examined. **Figure 4** shows the chemistry of PEG-4-Acrylate and images of the LCM cuts.

3.1.2 Alginate

Alginate (Sigma Aldrich A2033-100G) is a naturally occurring anionic polymer that has been investigated and used for biomedical applications along with other hydrogels. It can be prepared by various cross-linking methods. The most common method to prepare alginate utilizes an aqueous alginate solution combined with ionic cross-linking agents, such as divalent cations from calcium chloride. Like other hydrogels, with different crosslinking strategies, various chemical structures, molecular weights, and crosslinkers, mechanics and functionality can be tuned for applications.[25] Alginate compatibility and

ease of cutting were tested with LCM photoablation. The chemistry and LCM cuts are displayed in **Figure 4**.

3.1.3 *GelMA*

Gelatin Methacryloyl (GelMA, Sigma Aldrich 918628-1EA) is derived from gelatin and offers biocompatibility and tunable mechanical properties for various biomedical applications. GelMA crosslinking when exposed to light irradiation is referred to photoinitiated radical polymerization. GelMA polymerizes under UV light exposure with the presence of a water-soluble photoinitiator, commonly lithium acylphosphonate salt (LAP), to covalently crosslink. Physical parameters and characteristics of GelMA can be tuned by manipulating synthesis and processing. Mechanical properties, pore sizes, degradation rates, and swell ratio can be altered through changes in the degree of methacryloyl substitution, the concentration of the GelMA prepolymer, initiator concentration, and UV exposure time.[26] The chemistry of GelMA and the LCM cuts performed to test compatibility with photoablation is shown in **Figure 4**.

3.1.4 *Results and Weight Percentage*

There were considerable differences in the stability of hydrogels during and after laser photoablation. As shown in **Figure 4**, photoablation of PEG-Acrylate caused excessive bubble formation and photoablation of Alginate produced non-visible ablations. While maintaining the same LCM properties and settings and the same weight percent by volume, GelMA's performance with photoablation was superior to Alginate and PEG-Acrylate. As displayed in **Figure 4**, GelMA retained the cut shape, and the channel maintained its diameter when compared to Alginate and PEG-Acrylate. Therefore, GelMA

was the biomaterial of choice for future study. The integrity of GelMA compared to the other hydrogels given the same weight percentage can be attributed to the gelatin-based nature of GelMA. GelMA has a higher water retention capacity than Alginate and PEG-Acrylate. Gelatin possesses hydrophilic properties, allowing it to readily absorb and retain water within the hydrogel. PEG is a non-ionic polymer that exhibits low water absorption due to its hydrophobicity, and alginate, as a natural polysaccharide, exhibits relatively lower water retention than GelMA but higher than that of PEG. Water retention in all hydrogels can be influenced by many factors including concentration of monomer and

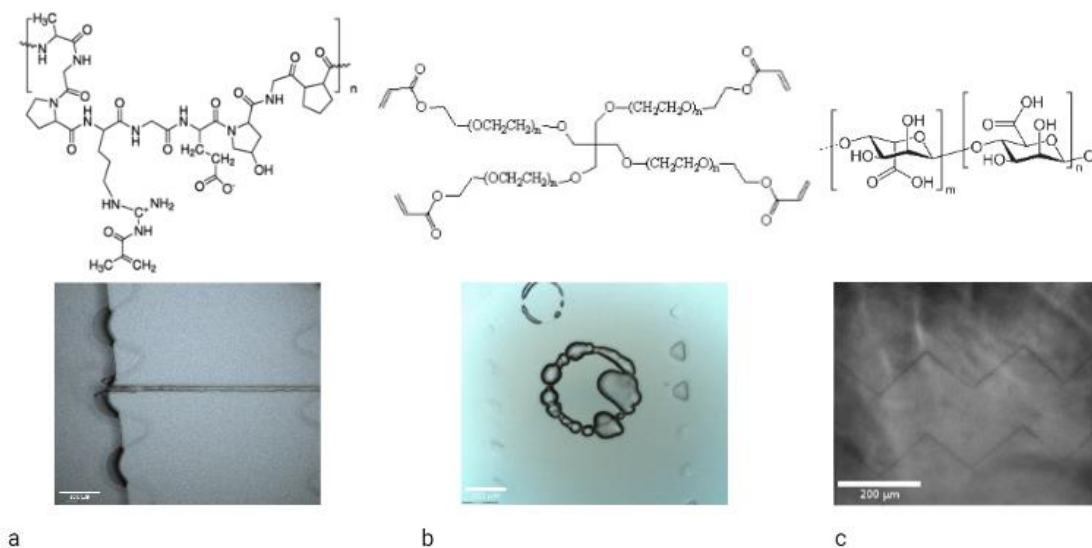


Figure 4 The chemical structures and associated photoablations of (a) GelMA, (b) PEG-4-Acrylate, and (c) Alginate. GelMA formed defined cuts, PEG-Acrylate formed bubbles, and Alginate did not respond to LCM ablations. The z-formation patterns in Alginate are cuts on the device, not the hydrogel itself showing incompatibility of Alginate with LCM.

crosslinking density. Laser photoablation functions through directed vaporization of material; therefore, due to GelMA's higher water retention property, GelMA seems more amenable to evaporation of water by LCM technology than the other hydrogels.

Controlled experimentation to determine the hydrogel of choice was performed at a consistent weight percentage. Weight percentage is a property that characterizes hydrogels and can be tuned by the concentration of monomer and other crosslinking properties. It plays a significant role in the stability and retention of laser cuts as well. Manipulation of weight percentage and the impact on photoablation was evaluated and discussed in later sections.

3.2 Microfluidic Device Design

Hydrogel was loaded into a microfluidic device to test laser photoablation of channels and perfusion through the channels. Microfluidic chip design that is conducive to LCM technology was determined. Device design was refined to two microfluidic devices that consist of three main reservoirs. Detailed methodology of the microfluidic device preparation and photoablation procedure are discussed in the Methods section, and the preparation as well as image of the devices are shown in **Figure 5**. Parameters of the laser photoablation, discussed in the Laser Cutting Optimization section, were troubleshooted and adjusted for each device. However, unlike for the hydrogels, the difference between optimal parameters for ablation for each of the devices was negligible. The settings utilized are listed in the following section.

3.2.1 Serpentine Device

One of the tested microfluidic designs consisted of three main reservoirs beside each other. The middle reservoir was enclosed by pillars designed to confine hydrogel loaded into that area. The inlets to the outer reservoirs beside the hydrogel-loaded reservoir are in the serpentine form. The serpentine channels begin as two inlets and branch into

multiple channels that feed into the outer reservoirs. The intended use of these serpentine patterns is to form a gradient throughout the three reservoirs perpendicular to the flow. All three reservoirs contain one channel on the other side of the serpentines for loading or discharge. This design is depicted in **Figure 5** with the dimensions of the main reservoirs shown in **Table 1**.

3.2.2 *Three-Channel device*

Another tested microfluidic design contained three channels of larger dimensions. The three channels acted as reservoirs. As with the serpentine device, the middle channel was bordered by pillars intended for hydrogel loading. The design is shown in **Figure 5** and the dimensions of the channels are given in **Table 1**.

3.2.3 *Results*

The effect of microfluidic device design on laser photoablation was explored. The serpentine device dimensions were advantageous for laser photoablation. The smaller reservoirs allowed for complete cuts that were less likely to reclose, and the width of the hydrogel-loaded channel was wide enough to permit cutting long channels or other patterns. Nevertheless, it was observed that longer laser cut channels lead to a higher likelihood that the hydrogel would retract back to its original shape and close the channel. The serpentine device minimizes this problem with a narrower hydrogel-loaded reservoir, which leads to a shorter laser cut channel. However, the serpentine device included gradient serpentine channels that were unnecessary and not useful for experimentation or laser photoablation. As shown in **Figure 5b**, the serpentine channels were connected independently from the reservoirs. This allowed for flow to and from the outer reservoirs

without the need to flow through the hydrogel-loaded channel. This caused difficulty in viewing perfusion through a laser photoablated channel or network without imaging.

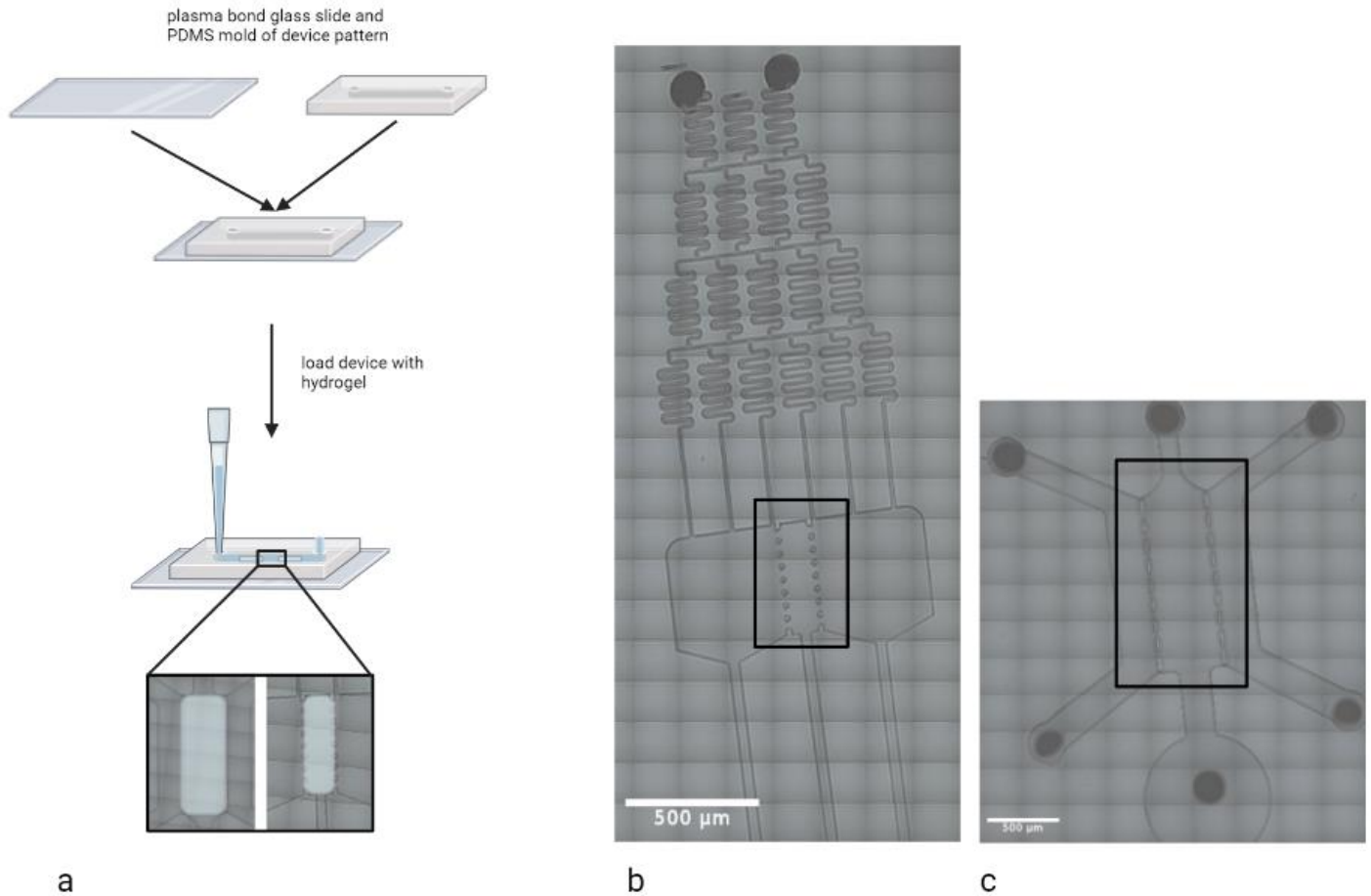


Figure 5 (a) Microfluidic device preparation procedure before performing photoablation. Tiled brightfield images of the microfluidic pattern design of the (b) Serpentine Device and (c) Three-Channel Device

The simple design of the three-channel device was more advantageous for experimentation, especially for perfusion testing. Compared to the serpentine device, perfusion from one of the outer reservoirs or channels to the opposite outer reservoir or channel was an indicator of perfusion through the channel or pattern. However, unlike the serpentine device, the dimensions of the channels in the three-channel device design were

less conducive to laser cutting. Both the width of the hydrogel channel and the depth were larger than the serpentine device. This caused the hydrogel to retract and close the laser cuts more often than cuts in the serpentine device. This is depicted in the **Appendix** that shows collapsed long cuts in the three-channel device. Both the serpentine device and the three-channel device were used for different experimental applications due to their advantages in different situations. This will be discussed further in the methodology.

Table 1 Microfluidic Device Dimensions

Device	Outer Reservoirs			Central Hydrogel Loaded Reservoir			Channels	
	Depth (μm)	Width (μm)	Height (μm)	Depth (μm)	Width (μm)	Height (μm)	Inlet Width (μm)	Outlet Width (μm)
Serpentine	100	421	416	100	122	416	35	20
Three-Channel	200	266	1215	200	452	1215	142 215	215

3.3 Laser Cutting Optimization

ZEISS PALM LCM technology consists of many settings and properties that were designed for cell population isolation from tissue samples. Therefore, setting optimizations were required for the purpose of hydrogel laser photoablation.

3.3.1 Microscope Properties

The LCM technology is composed of three major components: a high-resolution microscope, a laser microdissection device, and advanced software for precise targeting and control. The two components requiring manipulation and optimization were the microscope settings and the laser microscope settings. It was observed that laser

photoablation capabilities were significantly affected by the focus of the microscope. This was due to the establishment of a z-plane and target prior to laser ablation. The microscope focus and targeted z-plane changed for each device design and for each individual device. The process of LCM cutting of hydrogels included an optimization step for the microscope focus, which will be described in more detail in the methods section. Another setting that impacted laser photoablation was the choice of objective which determined the spatial resolution of the laser. The laser power was distributed over a greater area in the lower objectives (5x,10x) and more precise and targeted distribution of laser power in the higher objectives (20x, 40x). Thus, the laser cuts were wider in the lower objectives. The optimal objective used for all experiments was 10x which was consistently used in past studies as well.[21, 23]

3.3.2 Laser Properties

Properties of the laser microdissection device were the primary emphasis of optimization. There are two main functions that can be performed using LCM technology: cutting and catapulting. The only deviation between the two functions is a change in focus and power of the laser such that the sample would launch a section of the sample. While catapulting for the purpose of sample collection in a vial was not performed for the hydrogel experiments, the catapult setting was utilized in special cases of microchannel fabrication.

The major properties of the laser cutting function in the ZEISS PALM LCM system include laser energy, focus, cycle, and speed. All the settings were optimized such that the laser photoablation resulted in a well-defined, non-retractable channel or patterned network

within GelMA. Retractions and actively closing channels during photoablation is shown in the **Appendix**. Furthermore, settings were optimized to reduce large air bubble formations as depicted in the **Appendix**. The process by which optimization was done is discussed in detail in the methods section. The optimal settings are presented in **Table 2** and are specific to GelMA and the microfluidic designs discussed previously.

Table 2 Optimized Settings for ZEISS PALM LCM Technology

LCM Component	LCM Optimized Settings	
	PALM system designation	Associated Value
Laser Cut		
Energy (90 μ J Total)	70	63 μ J
Focus	90	-
Cycle	2-3	-
Speed	20	20 pulses/sec 2ns pulse duration
Laser Catapult		
Energy	75	67.5 μ J
Focus	90	-

The major properties of the laser catapulting function in the ZEISS PALM LCM system include laser catapult energy and catapult focus. The values, similar to the laser properties, were optimized to produce controlled ablation of the hydrogel. The optimal and specific settings are given in **Table 2** and the optimization process is discussed in detail in the methods section. The combination of cutting and catapulting was done to achieve the imputed pattern, clear definition, and proper width of channels.

CHAPTER 4. DEVELOPMENT OF LYMPHATIC VASCULATURE

After optimization of material and set-up, laser photoablation technology was used to mimic lymphatic vasculature. The goal was to exploit these methods to pattern lymphatic vasculature in both normal and malformed cases. The biomechanical properties of hydrogels were leveraged to mimic the in vivo microenvironment, and photoablation was utilized to pattern perfusable vessels that reflect the morphology of in vivo vasculature. The approach for each experiment followed three main steps: cut a pattern, test perfusion, and attempt flow of immune cells. As mentioned previously, perfusion was evaluated against two criteria: the reservoirs on each side of the channels or patterned networks are filled with influent, and the fluid was well-defined within the channels or conduits without leakage.

4.1 Weight percentage

Weight percentage is a major property that characterizes the hydrogel and has a significant impact on channel integrity upon laser photoablation. The weight percentage of GelMA was manipulated through variations in monomer concentration. A range of GelMA weight percentage from 5 wt/v% to 20 wt/v% was tested for compatibility with LCM and integrity of channel cuts. **Figure 6** depicts the variation of channels with different GelMA weight percentages in brightfield images with their respective dimensions described in **Table 3**. Confirmation of perfusion was performed using fluorescein isothiocyanate-

dextran (FITC). FITC was perfused through the microfluidic and given 30 minutes to flow through the LCM ablated channels. A pipette tip was filled with FITC and set in the device allowing FITC to flow through the device without added pressure of pipetting and disturbing the hydrogel. For a device without hydrogel, it takes approximately 30 minutes for the serpentine device to fill completely with FITC; therefore, this time standard was used for flow testing. This allowed for all conduits and channels to be filled as well. The images of the FITC through the channels at varying weight percentages are shown in **Figure 6**.

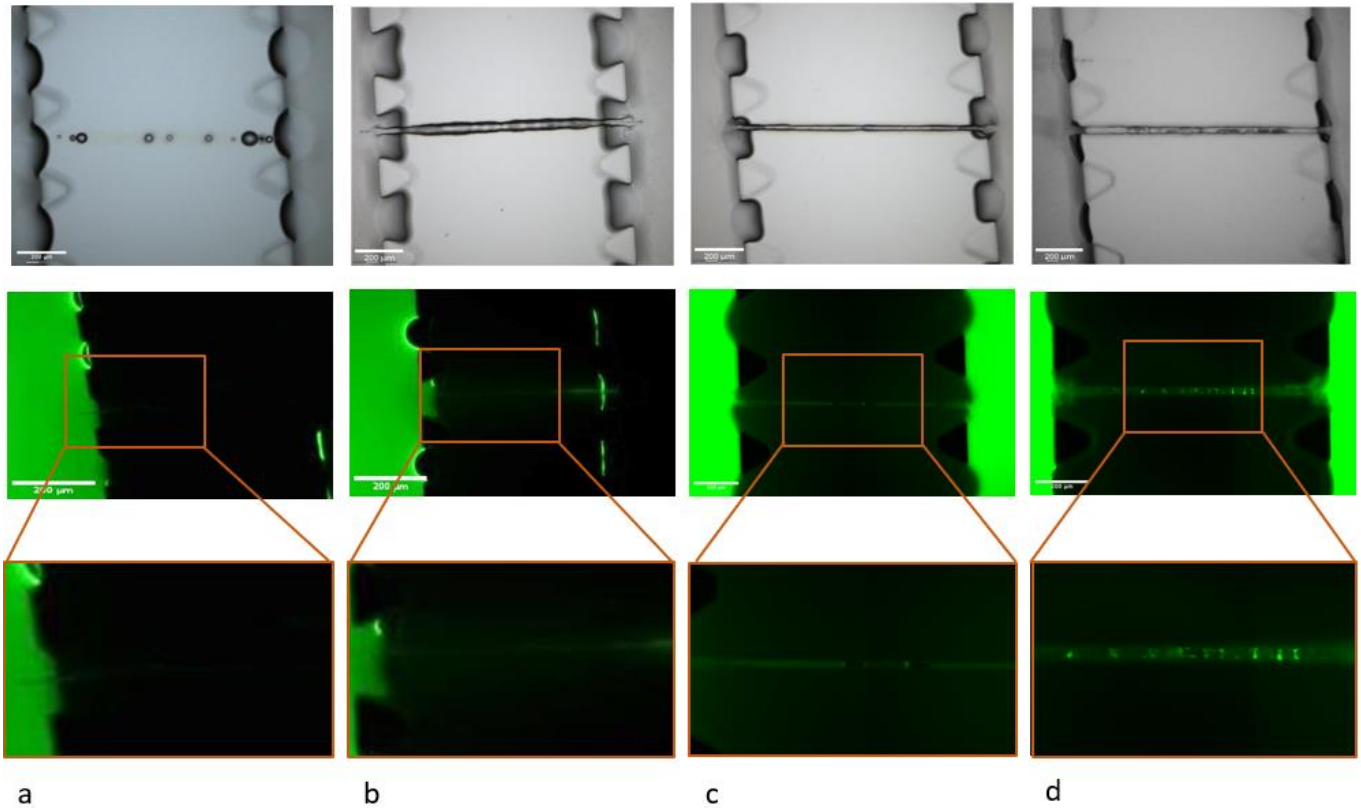


Figure 6 Brightfield images of laser ablated channels and perfusion of FITC through channels of GelMA at (a) 5 wt/v% (b) 10 wt/v% (c) 15 wt/v% and (d) 20 wt/v%

Table 3 Channel dimensions of laser ablated channels at varied GelMA weight percentage.

Weight percentage (wt/v%)	Channel Dimensions (μm)	
	Width	Length
5	0	0
10	20.8-36.8	836
15	14.5-18.5	994.5
20	21.0-26.0	1064.1

Weight percentage played a significant role in channel integrity. GelMA presented at low weight percentage, 5 wt/v% and 10 wt/v%, was more susceptible to reversion and closing of the channel. While 5 wt/v% showed FITC in the outer reservoirs, no perfusion was seen in the middle of the channel. Additionally, 10 wt/v % showed incomplete perfusion of FITC, and 15 wt/v % resulted in minimal perfusion of FITC with little FITC shown within the channel. This same effect was observed in the inlets and outlets of the channels at the location of the pillars bordering the central, hydrogel-loaded channel in the devices, regardless of the increasing weight percentage of the GelMA, further illustrated in the **Appendix**. The weight percentage at the edges of the hydrogel where inlets and outlets were laser ablated were possibly of lower weight percentage than the central portion of the hydrogel leading to reversion susceptibility. The weight percentage that presented this effect the least was 20 wt/v%, which is reflected by the channel definition as compared to the lower weight percentage GelMA cuts. Increasing weight percentage from 20 wt/v% caused a higher risk of hydrogel burning during hydrogel construction. Therefore, experimentation progressed by utilizing 20 wt/v% GelMA.

Swelling, a characteristic property of hydrogels, was a challenge for testing perfusion. Upon contact with fluids, hydrogels can swell significantly causing the same

reversion effect. This swelling also led to sealing the inlets and outlets thus rejecting perfusion through the channel. However, as weight percentage increased, the channels maintained integrity regardless of the swelling effect. This confirmed the progression utilizing 20 wt/v% GelMA. Perfusion was also confirmed using 3nm FITC coated beads through the LCM cut channels in 20 wt/v% GelMA and are presented in the subsequent section with a simple channel cut perfusion. FITC coated beads allowed for visualization of congregating populations within the conduits. Furthermore, beads allowed us to see if there is diffusion through the hydrogel matrix or leakage of beads from the channels or conduits into the hydrogel.

4.2 Channel Cuts

There were three main patterns laser cut using LCM technology and perfusion was tested in the same manner as the weight percentage experimentation. The detailed methods are described in the methods section.

4.2.1 Simple Channels

The weight percentage and perfusion experiment, as previously discussed, involved the creation of straight channels. Laser ablation was employed to generate these channels within a 20 wt/v% GelMA hydrogel. Subsequently, perfusion tests were conducted using FITC and FITC-coated beads. **Figure 7** displays the corresponding images, providing a visual representation of the cut dimensions documented in **Table 4**.

4.2.2 Branched Network

To progress towards creating a microcirculation model that emulates lymphatic systems, the subsequent phase involved laser cutting a more intricate pattern instead of a simple channel. Specifically, a branched channel design was sketched and subsequently ablated. The brightfield image capturing this structure, along with the perfusion test employing FITC-coated beads, is depicted in **Figure 7**. The dimensions of the branched network channel can be found in **Table 4**.

4.2.3 Lymphatic Channels

As stated in the background, lymphatic malformations manifest as bulb-like structures that emerge from the capillaries within the lymphatic vasculature. In an effort to replicate these formations, GelMA hydrogels were utilized alongside laser photoablation

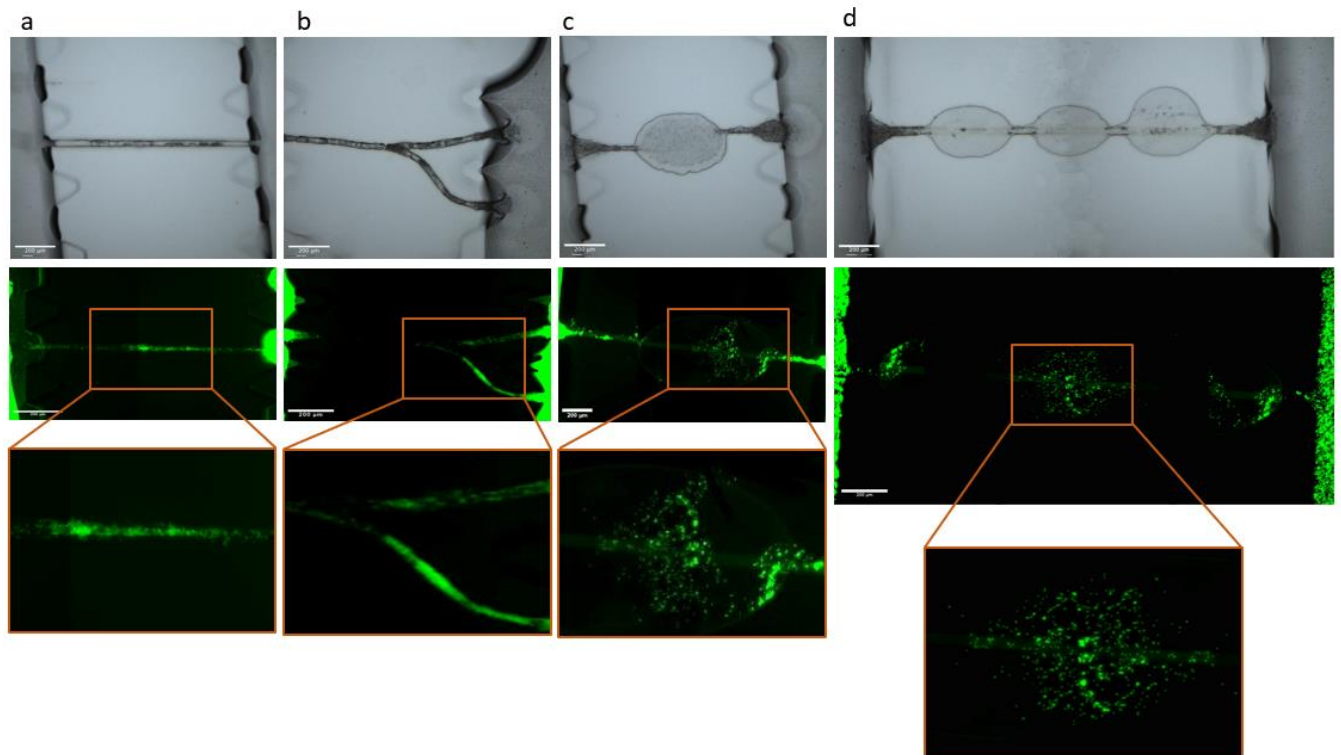


Figure 7 Various laser ablations at 20 wt/v% GelMA and associated perfusion with FITC coated beads through (a) simple channel, (b) branched channel, (c) single malformation channel, and (d) triple malformation channel.

where numerous designs featuring malformations were explored. The procedure for laser ablating the malformations is discussed in the Methods section. For the serpentine device design, ablations involving a single bulb were executed, taking advantage of the smaller dimensions of the central hydrogel-loaded channel. However, as the occurrence of malformations in individual channels or capillaries increased, the need for a new device design became evident. Consequently, the three-channel device was employed for multiple malformations, offering greater space within the central hydrogel-loaded reservoir. **Figure 7** showcases the brightfield images and perfusion tests using FITC-coated beads, while the corresponding dimensions of the malformations are outlined in **Table 4**.

Table 4 Dimensions of laser ablations of various cut designs

Cut Design	Dimensions of Photoablations (μm)							
	Bulb Width(s)	Branch Point Width	Connecting Channel Width(s)	Inlet Width	Outlet Width	Connecting Channel Length(s)	Bulb Length(s)	Total Length
Simple	-	-	26.1	27.1	25.0	-	-	1091.3
Branched	-	63.0	28.6	59.5	64.0	571.3	-	1779.8
			28.3		61.6	613.2		
			29.7			595.3		
Single Malformation	295.2	-	29.7	116.7	101.8	-	453.8	1048.2
Triple Malformation	246.0	-	38.2	180.2	144.2	123.4	419.8	2052.4
	241.7		25.4			92.6	394.4	
	333.0		38.1				409.2	
			29.7					

4.2.4 Perfusion with Cells

After confirmation of perfusion with beads, progression to the flow of cells through the channels was performed. Therefore, perfusion of B Lymphocytes, specifically Ly7 cells, labeled with Cell Tracker Red was conducted. Fluorescent images were captured 30

minutes after perfusion, similar to the experimentation of FITC perfusion. The cells were successfully perfused through a simple, straight channel and a single malformation pattern. A few cells were observed within the central region of each, demonstrating the capability of perfusion through laser microdissection (LCM) ablated conduits. This is indicated in **Figure 8**. Cells did not fill up the malformations as well as FITC and FITC beads in previous sections. Cells may have adhered to walls and were not free to move within the

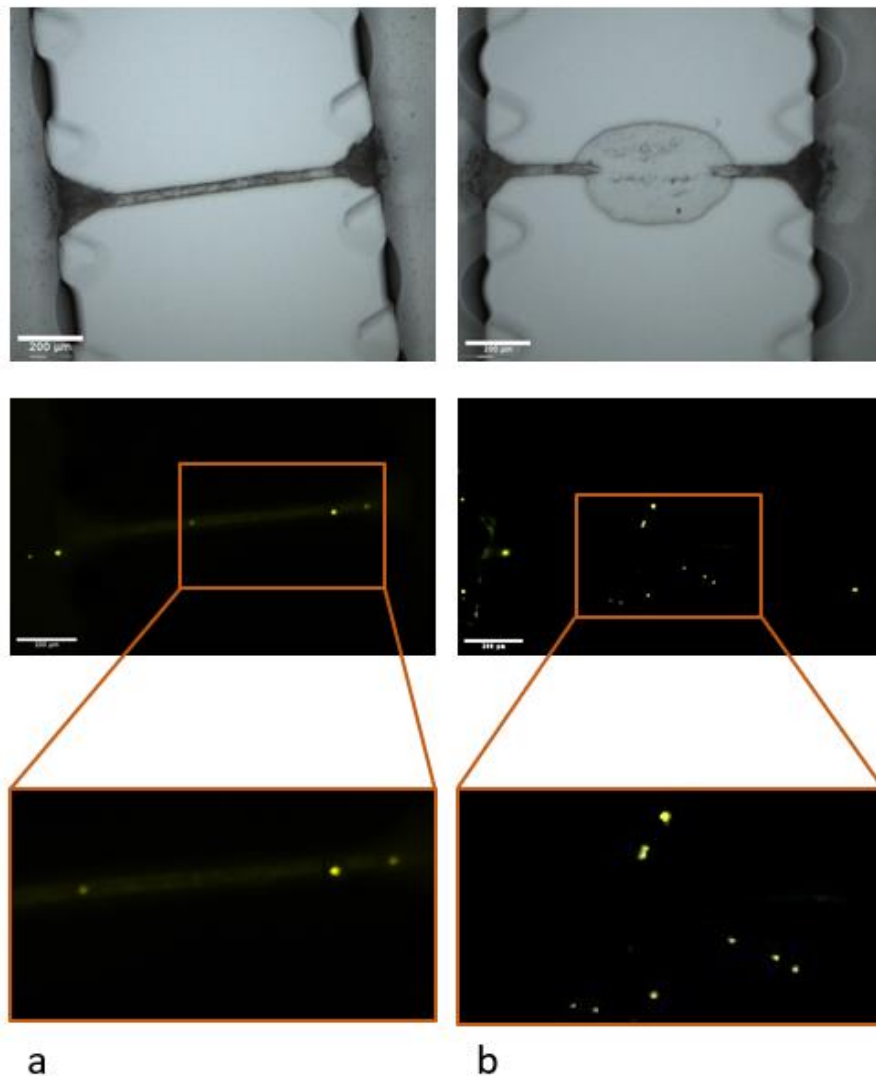


Figure 8 Perfusion of a (a) simple channel and (b) malformation with lymphocytes tagged with Cell Tracker Red and associated brightfield image of laser ablations.

channels or conduits. Although this does not confirm perfusion as evaluated by the study criteria, this opens the possibility of cells to enter photoablated patterns in hydrogel. Further study on conduit structure to allow immune cells to free flow through the interstitial space can be performed.

5.1 Hydrogel Preparation

The preparation of GelMA and the associated crosslinking process began with preparing the photoinitiator solution. 0.5 wt/v% photo initiator solution was prepared through the addition of LAP to PBS followed by heating and agitation at 60 °C for 20 minutes. Sigma Aldrich Low endotoxin GelMA is added and heated until fully dissolved (approximately 1-1.5 hours). Production of the desired wt/v% was determined through variation in GelMA monomer added to the solution. Hydrogels were prepared by pipetting the solution into microfluidic devices. A UV light station is set up, and the distance between the hydrogels and the UV source is measured using a UV light meter to determine the precise UV irradiance. For LAP, the hydrogels are exposed to 5 mW/cm² UV. After 30-40 seconds of UV exposure for crosslinking.

To prepare PEG-Acrylate, the hydrogel monomer, peptide ligand, and crosslinker aliquots were obtained. PEG-Acrylate and peptide aliquots were reconstituted with HEPES buffer. PEG-Acrylate, peptide ligand, and HEPES buffer were combined to create the ligand-macromer solution, termed mixture 1. After the solution had a PEG-Acrylate concentration double the desired concentration, had a maximum peptide-to-Acrylate ratio of 1:1, and had a volume 50% of the target volume, the mixture 1's pH was adjusted to 7.4 using 1M NaOH. It was incubated at 37°C for 30 minutes to functionalize PEG-Acrylate with the peptide ligand. For the crosslinker solution, termed mixture 2, Dithiothreitol (DTT), VPM peptide, and HEPES buffer were combined, ensuring a specific VPM to DTT molar ratio within 1:1 to 1:0, total molar concentration 1.5 times that of PEG-Acrylate, and

volume 40% of the target volume. Mixture 2's pH was adjusted to 5 using 1M NaOH or 1M HCl. The hydrogel was assembled by pipetting mixture 1 onto a glass slide, adding mixture 2 to the middle of the initial droplet, and gently mixing. Finally, the hydrogel was crosslinked by incubating the plate at 37°C for 15 minutes.

Alginate solution was prepared by dissolving alginate powder in phosphate-buffered saline (PBS) as a buffer to maintain the desired pH. The alginate solution was combined with the crosslinker, calcium chloride (CaCl₂) solution. The formation of a crosslinked gel occurred spontaneously. The alginate hydrogel shape was controlled to be a droplet on a glass slide.

5.2 Microfluidic Device Creation

Microfluidic devices given a prefabricated design were formulated by preparing polydimethylsiloxane (PDMS). Krayden Dow Sylgard 184 Silicone Elastomer Kit was used whereby a mix of the two components was poured into a device design mold and cured at 65°C for over 8 hours. If necessary, the devices were sterilized in an autoclave. The PDMS molds were plasma bonded onto glass slides. GelMA was pipetted into the central channels of each device and crosslinked as mentioned above and shown in **Figure 5**.

5.3 LCM

5.3.1 Optimization of Laser Cut and Catapult Settings

To perform cutting using the laser microdissection system, the microscope focus was adjusted to the desired depth and area of the sample. Then, necessary adjustments were

made to the laser energy, focus, and cycles to achieve precise cutting. Manual calibration was required, where an element was drawn and laser settings were adjusted during the cutting process. Laser energy and focus were increased while the laser was actively cutting until a well-defined ablation was seen as shown in the channel ablations in **Figure 6**. Cycles were increased to enhance definition and widen the conduits in hydrogel samples. The optimal settings of laser energy, focus, and cycles were recorded for future reference. However, it was worth noting that optimizing cutting settings specifically for cuts within a hydrogel required separate experimentation and adjustment. Optimization of laser settings particular to GelMA was performed. Due to variations in devices, adjustment of microscope settings was performed while maintaining laser settings specific for GelMA.

Laser cutting and catapulting was performed to achieve the lymphatic malformation cuts. The same procedure to optimize settings for laser energy and focus were done to obtain optimal settings for catapult energy and focus. Optimization of settings of the laser cutting and settings of the laser catapult were done at the same microscope focus on GelMA so that there was consistency between the two ablation methods. After all settings were optimized, listed in **Table 2**, the values were recorded and utilized for all experiments only changing the microscope focus for each device due to variation in devices.

5.3.2 LCM Cutting and Perfusion Procedure

Laser photoablation was performed with laser cutting, laser catapulting, or a combination of both. Sigma Aldrich FITC and 3 μ m FITC-marked Microparticles based on melamine resin were used to test perfusion through laser-ablated patterns. One reservoir

was loaded with FITC or beads with a pipette tip leading to flow through the laser cut channels.

Perfusion with Ly7 cells, an immortalized human B-cell lymphoma cell line, was conducted on laser-ablated conduits. After the cells were cultured to obtain sufficient seeding density, Ly7 cells were stained with Cell Tracker Red. The cell solution was then pipetted into one reservoir and perfusion was tested similarly to the experimentation with FITC perfusion.

CHAPTER 6.

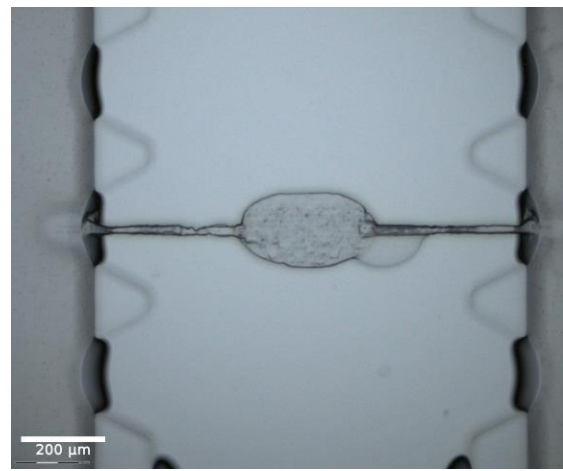
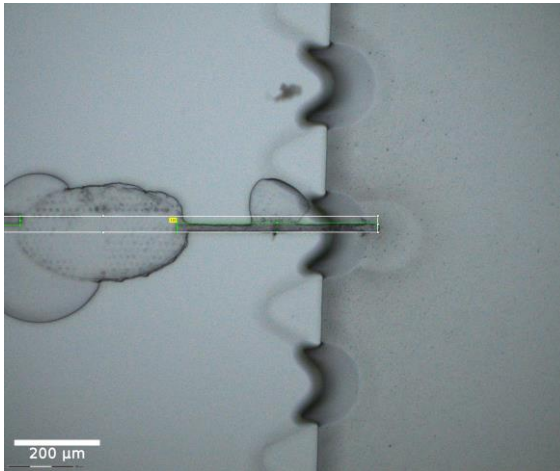
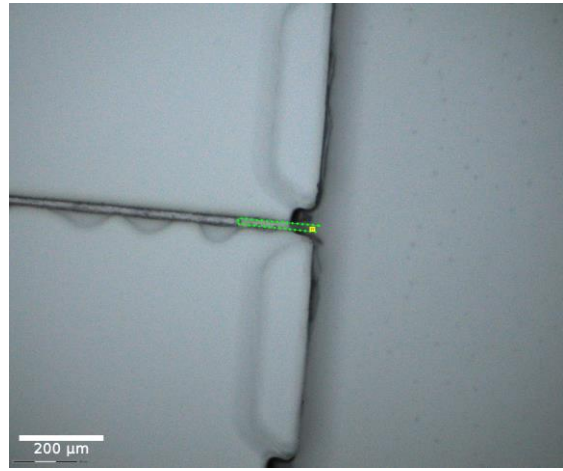
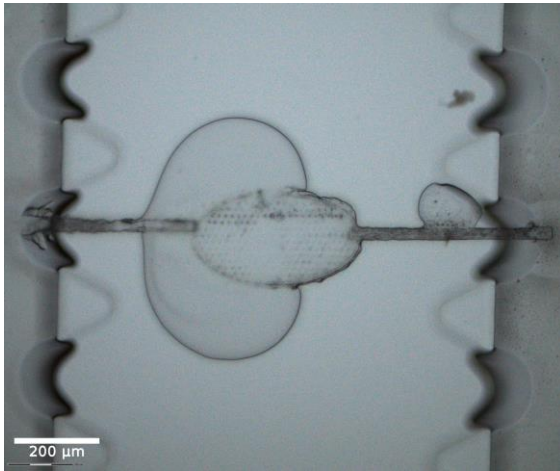
CONCLUSIONS AND FUTURE

DIRECTIONS

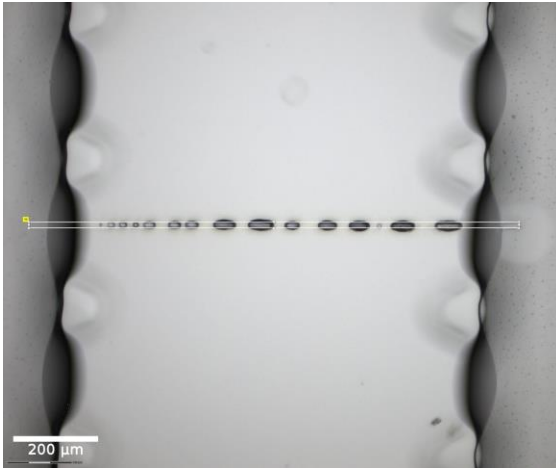
The utilization of LCM technology presents numerous possibilities for various applications in modeling lymphatic and other vasculature. The ability to vary the patterns of cuts allows for the representation of both normal and abnormal morphologies, enabling modeling of both healthy and pathological states. To further enhance future modeling endeavors, exploring alternative hydrogels would likely prove beneficial. Additionally, next steps should involve developing extended patterning and more sophisticated networks that enable perfusion, applicable to both 2-dimensional and 3-dimensional vasculature models. Development of intricate patterns would provide a platform to flow cells, particularly endothelial cells, through the channels to form endothelialized lumens. Hydrogels provide the added benefit of a matrix for embedding cells or molecules that could interact with the modeled capillaries and lymphatics. Consequently, applications arise in the domains of tissue engineering, system or organ-on-chip platforms, and organoid models.

APPENDIX A. SUPPLEMENTAL IMAGES

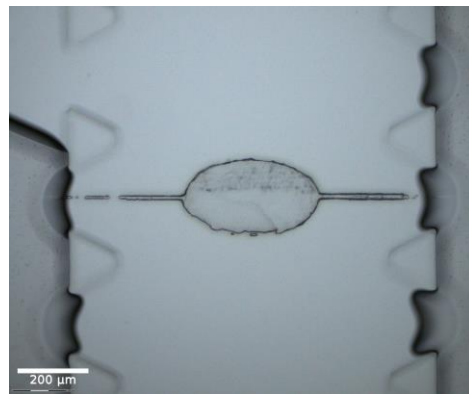
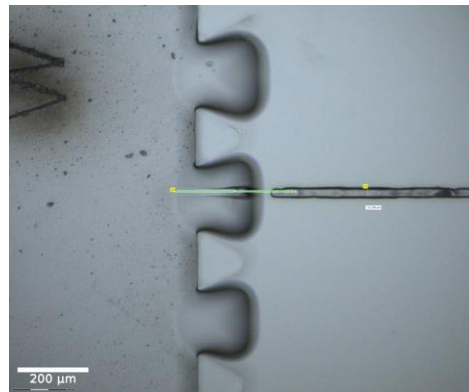
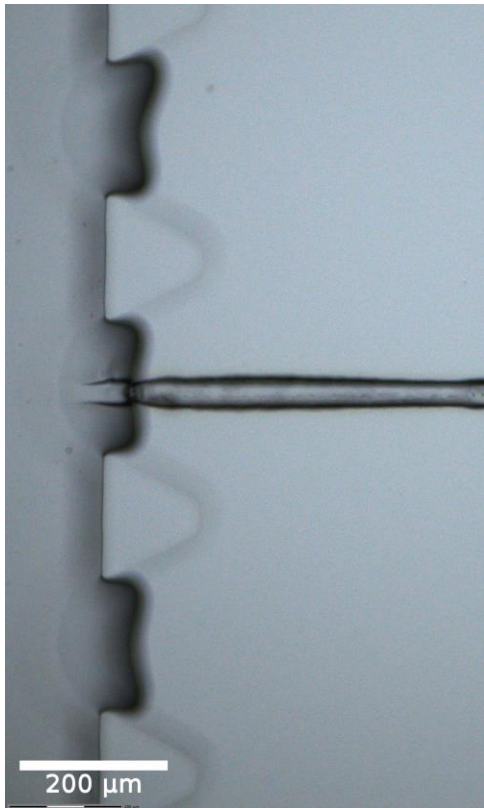
A.1 Bubble Formation during Photoablation Process



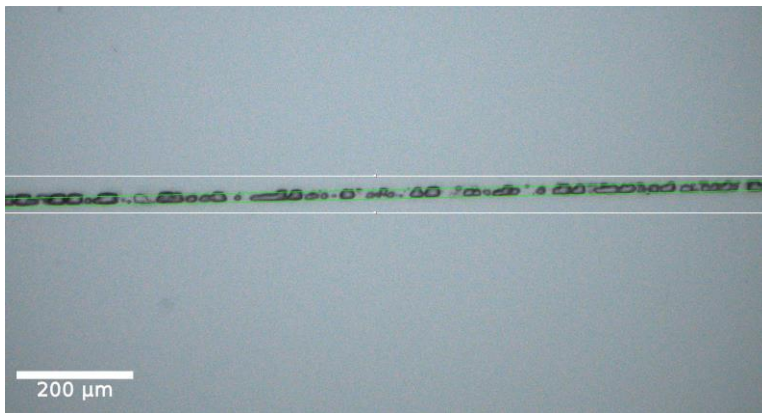
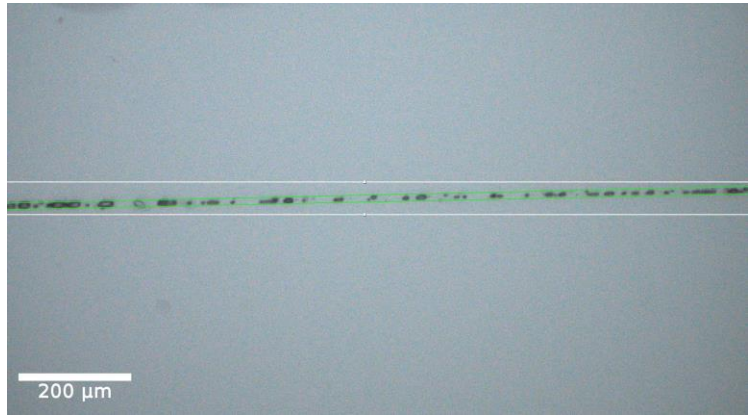
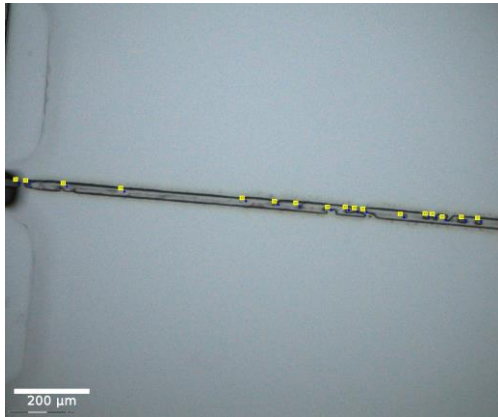
A.2 Channel Closing during Photoablation Process



A.3 Inlet and Outlet Close during Photoablation Process



A.4 Long Laser Cuts in Three-Channel Device During Photoablation Process



REFERENCES

1. Randolph, G.J., et al., *The Lymphatic System: Integral Roles in Immunity*. Annu Rev Immunol, 2017. **35**: p. 31-52.
2. Swartz, M.A., *The physiology of the lymphatic system*. Advanced Drug Delivery Reviews, 2001. **50**(1-2): p. 3-20.
3. Oliver, G., *Lymphatic vasculature development*. Nature Reviews. Immunology, 2004. **4**(1): p. 35-45.
4. Steele, M.M. and A.W. Lund, *Afferent Lymphatic Transport and Peripheral Tissue Immunity*. J Immunol, 2021. **206**(2): p. 264-272.
5. Makinen, T., et al., *Lymphatic Malformations: Genetics, Mechanisms and Therapeutic Strategies*. Circ Res, 2021. **129**(1): p. 136-154.
6. Petkova, M., et al., *Immune-interacting lymphatic endothelial subtype at capillary terminals drives lymphatic malformation*. Journal of Experimental Medicine, 2023. **220**(4).
7. Greene, A.K., C.A. Perlyn, and A.I. Alomari, *Management of Lymphatic Malformations*. Clinics in Plastic Surgery, 2011. **38**(1): p. 75-82.
8. Selahi, A. and A. Jain, *Engineered models of the lymphatic vascular system: Past, present, and future*. Microcirculation, 2023. **30**(2-3): p. e12793.
9. Luque-Gonzalez, M.A., et al., *Human Microcirculation-on-Chip Models in Cancer Research: Key Integration of Lymphatic and Blood Vasculatures*. Adv Biosyst, 2020. **4**(7): p. e2000045.
10. Henderson, A.R., H. Choi, and E. Lee, *Blood and Lymphatic Vasculatures On-Chip Platforms and Their Applications for Organ-Specific In Vitro Modeling*. Micromachines (Basel), 2020. **11**(2).
11. Campbell, K.T. and E.A. Silva, *Biomaterial Based Strategies for Engineering New Lymphatic Vasculature*. Adv Healthc Mater, 2020. **9**(18): p. e2000895.
12. Li, X., Y. Shou, and A. Tay, *Hydrogels for Engineering the Immune System*. Advanced NanoBiomed Research, 2021. **1**(3): p. 2000073.
13. Hooks, J.S.T., et al., *Synthetic hydrogels engineered to promote collecting lymphatic vessel sprouting*. Biomaterials, 2022. **284**: p. 121483.

14. Campbell, K.T. and E.A. Silva, *Biomaterial Based Strategies for Engineering New Lymphatic Vasculature*. *Advanced Healthcare Materials*, 2020. **9**(18): p. 2000895.
15. Dai, T.t., et al., *Reconstruction of lymph vessel by lymphatic endothelial cells combined with polyglycolic acid scaffolds: A pilot study*. *Journal of Biotechnology*, 2010. **150**(1): p. 182-189.
16. Knezevic, L., et al., *Engineering Blood and Lymphatic Microvascular Networks in Fibrin Matrices*. *Frontiers in Bioengineering and Biotechnology*, 2017. **5**.
17. Bonvin, C., et al., *A multichamber fluidic device for 3D cultures under interstitial flow with live imaging: Development, characterization, and applications*. *Biotechnology and Bioengineering*, 2010. **105**(5): p. 982-991.
18. Ayuso, J.M., et al., *Human Tumor-Lymphatic Microfluidic Model Reveals Differential Conditioning of Lymphatic Vessels by Breast Cancer Cells*. *Adv Healthc Mater*, 2020. **9**(3): p. e1900925.
19. Henderson, A.R., I.S. Ilan, and E. Lee, *A bioengineered lymphatic vessel model for studying lymphatic endothelial cell-cell junction and barrier function*. *Microcirculation*, 2021. **28**(8): p. e12730.
20. Espina, V., et al., *Laser-capture microdissection*. *Nature Protocols*, 2006. **1**(2): p. 586-603.
21. Brandenburg, N. and M.P. Lutolf, *In Situ Patterning of Microfluidic Networks in 3D Cell-Laden Hydrogels*. *Adv Mater*, 2016. **28**(34): p. 7450-6.
22. Sarig-Nadir, O., et al., *Laser Photoablation of Guidance Microchannels into Hydrogels Directs Cell Growth in Three Dimensions*. *Biophysical Journal*, 2009. **96**(11): p. 4743-4752.
23. Nikolaev, M., et al., *Homeostatic mini-intestines through scaffold-guided organoid morphogenesis*. *Nature*, 2020. **585**(7826): p. 574-578.
24. Parlato, M., et al., *Poly(ethylene glycol) hydrogels with adaptable mechanical and degradation properties for use in biomedical applications*. *Macromol Biosci*, 2014. **14**(5): p. 687-98.
25. Lee, K.Y. and D.J. Mooney, *Alginate: properties and biomedical applications*. *Prog Polym Sci*, 2012. **37**(1): p. 106-126.
26. Yue, K., et al., *Synthesis, properties, and biomedical applications of gelatin methacryloyl (GelMA) hydrogels*. *Biomaterials*, 2015. **73**: p. 254-71.